Journal of Control, Automation and Electrical Systems (2020) 31:636–647
https://doi.org/10.1007/s40313-020-00566-z

Control of a BDFIG Based on Current and Sliding Mode Predictive Approaches

Alix Dountio Tchioffo[1] · Eric Duckler Kenmoe Fankem[1] · Guidkaya Golam[1] · Martin Kamta[2] · Joseph Yves Effa[1]

Received: 9 September 2019 / Revised: 16 December 2019 / Accepted: 7 January 2020 / Published online: 27 January 2020

Abstract

The Brushless Doubly Fed Induction Generator (BDFIG) is a great attraction nowadays thanks to its high reliability and high low voltage ride-through capability. In variable speed generation systems, the most used control techniques are the vector control, direct torque/power control. Vector control is highly sensitive to parameters variations, while the two others offer high amount of ripples reducing power quality. This paper therefore proposes a Sliding Mode Power Predictive Control (SMPPC) and an Indirect Model Power Predictive Control (I-MPPC) for a simple and efficient power control of the BDFIG. The SMPPC takes current components in the $\alpha\beta$ frame as sliding surfaces derived from the I-MPPC based on current predictions to track the desired active and reactive powers in the BDFIG. A cost function defined as currents' quadratic errors is used to choose the appropriate voltage vector for control winding supply, and the Particle Swarm Optimization algorithm is used to determine the optimal gain for the SMPPC. Simulations on MATLAB/Simulink are carried out to show the effectiveness of the control schemes as well as their robustness to some parameters variations. More so, power compensation is used to improve the capability of the control strategy to provide sinusoidal and balanced currents under unbalanced grid conditions. The proposed methods compared to direct power control show good performances in terms of total harmonic distortion reduction, low ripples and robustness, strengthening the idea of using the BDFIG as an alternative to new generation of wind energy conversion systems.

Keywords Brushless Doubly Fed Induction Generator · Current prediction · Sliding mode control · Power compensation · Unbalanced grid

List of Symbols

R_p, R_c, R_r	Power winding, control winding, rotor resistance
L_{sp}, L_{sc}, L_r	Power winding, control winding, rotor self-inductance
M_p, M_c	Power winding, control winding mutual inductance with rotor
V_{sp}, V_{sc}, V_r	Power winding, control winding, rotor voltage
I_{sp}, I_{sc}, I_r	Power winding, control winding, rotor current
φ_{sp}, φ_{sc}, φ_r	Power winding, control winding, rotor flux
T_e, T_r	Electromagnetic, load torque
J, f	Inertia, friction coefficient
P, Q	PW active, reactive power

Subscripts

sp, sc, r	Stator power winding, stator control winding, rotor
*	Conjugate

1 Introduction

The rush to cheapest and more reliable sources of energy for power supply is a great challenge and even a necessity nowadays. Among these types of energy, wind energy occupies a crucial place (Sergio et al. 2016; Xiaoyu et al. 2018) thanks to the development of power electronics and electrical manufacturing machines. In variable speed operation schemes, wind energy conversion systems (WECS) are mainly driven by Doubly Fed Induction Generators (DFIG) (Ming and Yiing 2014; Saber et al. 2018). Nonetheless, one of its main drawbacks is the cost of maintenance actions

✉ Joseph Yves Effa
yveseffa@gmail.com

[1] Faculty of Science, University of Ngaoundere, Ngaoundere, Cameroon

[2] National School of Agro-Industrial Sciences, University of Ngaoundere, Ngaoundere, Cameroon

due to the presence of brushes and rings especially when offshore. In order to solve this issue, investigations are made on brushless machines, and as a result, the Brushless Doubly Fed Induction Machine (BDFIM) could be a good candidate (Henk et al. 2013; Tim et al. 2016). In fact, compared to a DFIG of same rate, the Brushless Doubly Fed Induction Generator (BDFIG) freed of brushes is more robust and reliable. It also has an improved low voltage ride-through capability and, due to its pole pair numbers, appears to be a medium speed drive candidate (Francisco et al. 2009; Shiyi et al. 2009; Henk et al. 2013; Tim et al. 2016).

To fulfil required conditions of operation in WECS, the BDFIG has to be under a good control strategy. Therefore, tremendous control strategies for the BDFIG have already been carried out. One can cite the most used technique to control electrical machines in practice known as vector control (VC), which has been investigated (Shiyi et al. 2009; Javier et al. 2009; Shiyi et al. 2013; Jiansheng et al. 2015).

However, VC needs rotary transformation, appropriate decoupling and proper adjustment of controller parameters to guarantee a fitting stability of the system over the whole operating range (Maryam et al. 2016; Xinchi et al. 2017). Moreover, the implementation of VC appears to be complicated and time-consuming (Xuan et al. 2017). In addition to VC strategies commonly used, there are the direct torque control (DTC) and direct power control (DPC) methods which are used to manage the complexity of VC, based on the selection of a voltage vector predefined in a lookup table (LUT), selections which are not usually the best ones and subject to significant ripples.

More so, LUT in field-programmable gate array (FPGA), for example, could be affected due to its propensity to be subject to faults (Hadi and Hanieh 2017). All these reasons therefore lead us to think of other control techniques for the BDFIM. In this light, to strengthen the capability of the BDFIM as an alternative to the conventional DFIG, sliding mode control (SMC) has also been investigated for its control (Jiabing et al. 2010; Mohamed et al. 2017; Guanguan et al. 2017; Ramtin et al. 2018). Although SMC strategies are known to be very robust and fast, their stability are not always guarantee at a finite time and they are subject to chattering effect (Ramtin et al. 2018).

In addition, a given wind power generation system has to cope with unbalanced grid condition which can occur in order to fulfil some grid code requirements. Hence, the behaviour of the BDFIG has to be investigated under unbalanced grid conditions. This is very important, for example in developing countries where grids are generally weak (Gonzalo et al. 2010), and could therefore be severely affected in terms of efficiency as well as loads too (Jianping et al. 2018). In fact, unbalanced grid conditions can occur on a WECS due to unsymmetrical loads, transformer windings or transmission impedance and transitory faults (Eduard et al. 1999; David et al. 2008). This can lead to non-sinusoidal currents responsible of heating on stator PW and/or additional stress on the rotor shaft due to torque oscillation. In that sense, vector controls are proposed in Shiyi et al. (2013) and Jiansheng et al. (2015) with the study of the BDFIG in unbalanced grid condition with three and four targets, respectively. In Jiefeng et al. (2014), power compensation with DPC is used to obtain sinusoidal currents under unbalanced grid conditions.

With the capacity of calculators nowadays, lesser time and space lickerish control techniques are needed to ensure a good control of electrical machines and BDFIG for instance. To do so, it has been shown in Venkata et al. (2015) that the predictive control is a good candidate and exists in different types among which the model predictive control (MPC) is the best one (Jose and Patricio 2012). A predictive control technique has no need for linear regulators or modulators (Venkata et al. 2015). It uses the plant system model to predict the behaviour of the controlled variables, and in some cases like in MPC, nonlinearity of the system can be introduced in the model (Jose and Patricio 2012; Xinchi et al. 2017) leading to a control scheme giving good results. The presentation of the Model Power Predictive Control (MPPC) on a Brushless Doubly Fed Twin Stator Induction Generator (BFTSIG) has been made in Xinchi et al. (2017) to show how effective the method can be in terms of dynamic performances and ripples reduction. This paper therefore steps forward to investigate power control of the BDFIG by proposing the so-called Sliding Mode Power Predictive Control (SMPPC) via an Indirect Model Power Predictive Control (I-MPPC) based on current prediction to achieve a simple and accurate control of active and reactive powers which are current images. This is motivated by the fast dynamics of currents and their sensors which are widely used in practice. A Particle Swarm Optimization (PSO) algorithm is used to determine the optimal gain necessary for fitting the stability and fast convergence of the SMPPC. To evaluate its performance, comparisons with the DPC applied on the BDFIG are carried out. Aside, power compensation in Jiefeng et al. (2014) is used to overcome the unbalanced voltage issue when present. The paper is organized as follows: Sect. 2 is dedicated to BDFIG's description and modelling. In Sect. 3, the proposed control schemes are presented as well as the PSO algorithm, while in Sect. 4, simulation results made of step changes, tests of robustness under speed and some parameters variation are carried out and the behaviour of the BDFIG with SMPPC and I-MPPC under unbalanced grid condition is investigated using an existing power compensation method to overcome it.

2 Machine Description and Modelling

2.1 Description

Invented in the mid-eighties at Oregon State University, the Brushless Doubly Fed Induction Machine (BDFIM) is a machine made up of two-stator windings which has been widely studied (Stephen et al. 1997; Richard et al. 2006; Tohidi 2016). The BDFIM is an induction machine that can operate in the asynchronous and the synchronous mode, the latter being the best.

2.2 Machine Modelling

As aforementioned, the synchronous mode is the most appropriate for the BDFIM in which the shaft speed is not directly linked to the torque and is expressed as follows:

$$\omega_r = \frac{\omega_p + \omega_c}{p_p + p_c} \tag{1}$$

where ω_r is the mechanical shaft speed, ω_p the PW's angular frequency and ω_c the CW's angular frequency.

In order to describe the behaviour of the machine, equations will be based on the works of Javier et al. (2006). The unified model of the machine in a generic dq axis is thus given by the following Eqs. (2) to (9):

$$\boldsymbol{V_{sp}} = R_{sp}\boldsymbol{I_{sp}} + \frac{\mathbf{d}}{\mathbf{d}t}\boldsymbol{\varphi_{sp}} + j\omega_a\boldsymbol{\varphi_{sp}} \tag{2}$$

$$\boldsymbol{V_{sc}} = R_{sc}\boldsymbol{I_{sc}} + \frac{\mathbf{d}}{\mathbf{d}t}\boldsymbol{\varphi_{sc}} + j(\omega_a - (p_p + p_c)\omega_r)\boldsymbol{\varphi_{sc}} \tag{3}$$

$$\boldsymbol{V_r} = R_r\boldsymbol{I_r} + \frac{\mathbf{d}}{\mathbf{d}t}\boldsymbol{\varphi_r} + j(\omega_a - p_p\omega_r)\boldsymbol{\varphi_r} \tag{4}$$

$$\boldsymbol{\varphi_{sp}} = L_{sp}\boldsymbol{I_{sc}} + M_p\boldsymbol{I_r} \tag{5}$$

$$\boldsymbol{\varphi_{sc}} = L_{sc}\boldsymbol{I_{sc}} + M_c\boldsymbol{I_r} \tag{6}$$

$$\boldsymbol{\varphi_r} = L_r\boldsymbol{I_r} + M_p\boldsymbol{I_p} + M_c\boldsymbol{I_c} \tag{7}$$

$$T_e = \frac{3}{2}p_p Im\left(\boldsymbol{\varphi_{sp}^*} \cdot \boldsymbol{I_{sp}}\right) + \frac{3}{2}p_c Im\left(\boldsymbol{\varphi_{sc}^*} \cdot \boldsymbol{I_{sc}}\right) \tag{8}$$

$$J\frac{\mathrm{d}}{\mathrm{d}t}\omega_r = T_e - T_r - f\omega_r \tag{9}$$

Intentionally, the vector sign on complex quantities is replaced by the quantities written in bold to ease the reading.

In Eq. (4), $\boldsymbol{V_r} = 0$. Equations (8) and (9), respectively, represent the electrical torque and the differential equation giving the mechanical speed. The angular speed of the unified reference frame ω_a is chosen according to the orientation of one of the three fluxes.

3 Proposed Control Schemes

3.1 BDFIG Model for Predictive Control

Based on PW flux orientation, the stationary $\alpha\beta$ frame (where $\omega_a = \omega_p = 0$) is used for the description of the BDFIG. On that assumption, Eqs. (2) to (4) become:

$$\boldsymbol{V_{sp}} = R_{sp}\boldsymbol{I_{sp}} + \frac{\mathbf{d}}{\mathbf{d}t}\boldsymbol{\varphi_{sp}} \tag{10}$$

$$\boldsymbol{V_{sc}} = R_{sc}\boldsymbol{I_{sc}} + \frac{\mathbf{d}}{\mathbf{d}t}\boldsymbol{\varphi_{sc}} - j\left(p_p + p_c\right)\omega_r\boldsymbol{\varphi_{sc}} \tag{11}$$

$$\boldsymbol{V_r} = R_r\boldsymbol{I_r} + \frac{\mathbf{d}}{\mathbf{d}t}\boldsymbol{\varphi_r} - jp_p\omega_r\boldsymbol{\varphi_r} \tag{12}$$

From Eqs. (5) to (7), the following relation can be written:

$$\begin{bmatrix} \boldsymbol{I_{sp}} \\ \boldsymbol{I_{sc}} \\ \boldsymbol{\varphi_{sp}} \end{bmatrix} = K\begin{bmatrix} K_{11} & K_{12} & K_{13} \\ K_{21} & K_{22} & K_{23} \\ K_{31} & K_{32} & K_{33} \end{bmatrix}\begin{bmatrix} \boldsymbol{\varphi_{sp}} \\ \boldsymbol{\varphi_{sp}} \\ \boldsymbol{\varphi_r} \end{bmatrix} \tag{13}$$

where K and K_{ij} ($i = 1, 3$ and $j = 1, 3$) are given in "Appendix A".

Choosing I_{sp}, I_{sc} and φ_{sp} as state variables, the machine model can be written in the following form:

$$\begin{bmatrix} \dot{\boldsymbol{I}}_{\mathbf{sp}} \\ \dot{\boldsymbol{I}}_{\mathbf{sc}} \\ \dot{\boldsymbol{\varphi}}_{\mathbf{sp}} \end{bmatrix} = \begin{bmatrix} \epsilon_{11} & \epsilon_{12} & \epsilon_{13} \\ \epsilon_{21} & \epsilon_{22} & \epsilon_{23} \\ \epsilon_{31} & \epsilon_{32} & \epsilon_{33} \end{bmatrix}\begin{bmatrix} \boldsymbol{I_{sp}} \\ \boldsymbol{I_{sc}} \\ \boldsymbol{\varphi_{sp}} \end{bmatrix} + \begin{bmatrix} \boldsymbol{\varepsilon}_{11} & \boldsymbol{\varepsilon}_{12} & \boldsymbol{\varepsilon}_{13} \\ \boldsymbol{\varepsilon}_{21} & \boldsymbol{\varepsilon}_{22} & \boldsymbol{\varepsilon}_{23} \\ \boldsymbol{\varepsilon}_{31} & \boldsymbol{\varepsilon}_{32} & \boldsymbol{\varepsilon}_{33} \end{bmatrix}\begin{bmatrix} \boldsymbol{V_{sp}} \\ \boldsymbol{V_{sc}} \\ 0 \end{bmatrix} \tag{14}$$

with the elements ϵ_{ij} and ε_{ij} given in "Appendix B".

3.2 Indirect Model Power Predictive Control

The control scheme we are presenting uses current prediction to constrain the machine to produce the desired powers (from which the active and the reactive powers are deduced). Hence, instead of directly controlling the active and reactive powers, these will be controlled through PW windings' current. To follow the desired active and/or reactive power, only the corresponding current needs to be tracked and it has been previously evaluated since the PW voltage is assumed to be fixed by the grid.

To present the control scheme, let's express the complex apparent power $\boldsymbol{S_p}$ in the PW fed by a three-phase grid by

$$\boldsymbol{S}_{\mathbf{p}} = \frac{3}{2}\boldsymbol{V}_{\mathbf{sp}}\boldsymbol{I}^{*}_{\mathbf{sp}} = P_{\mathrm{p}} + jQ_{\mathrm{p}} \tag{15}$$

where P_{p} and Q_{p} are the active and reactive powers.

The differentiation with respect to time of Eq. (15) leads to Eq. (16):

$$\frac{\mathbf{d}\boldsymbol{S}_{p}}{\mathbf{d}t} = \frac{3}{2}\frac{\mathbf{d}\boldsymbol{V}_{\mathbf{sp}}}{\mathbf{d}t}\boldsymbol{I}^{*}_{\mathbf{sp}} + \frac{3}{2}\frac{\mathbf{d}\boldsymbol{I}^{*}_{\mathbf{sp}}}{\mathbf{d}t}\boldsymbol{V}_{\mathbf{sp}} \tag{16}$$

In fact, the reference apparent power is defined as follows according to Eq. (15) given a constant PW voltage as previously assumed:

$$\boldsymbol{S}_{\mathbf{pref}} = \frac{3}{2}\boldsymbol{V}_{\mathbf{sp}}\boldsymbol{I}^{*}_{\mathbf{spref}} = P_{\mathbf{p}_{\mathbf{ref}}} + j\boldsymbol{Q}_{\mathbf{p}_{\mathbf{ref}}} \tag{17}$$

Therefore, the deduction of the reference current utterances in the $(\boldsymbol{\alpha}, \boldsymbol{\beta})$ frame can be done as follows:

$$I_{\mathbf{sp}\alpha_{\mathbf{ref}}} = \left(\frac{3}{2}\right)\left(\frac{P_{p_{\mathbf{ref}}}V_{\mathbf{sp}\alpha} + Q_{\mathbf{p}_{\mathbf{ref}}}V_{\mathbf{sp}\beta}}{V^{2}_{\mathbf{sp}\alpha} + V^{2}_{\mathbf{sp}\beta}}\right) \tag{18}$$

$$I_{\mathbf{sp}\beta_{\mathbf{ref}}} = \left(\frac{3}{2}\right)\left(\frac{P_{\mathbf{p}_{\mathbf{ref}}}V_{\mathbf{sp}\beta} - Q_{\mathbf{p}_{\mathbf{ref}}}V_{\mathbf{sp}\alpha}}{V^{2}_{\mathbf{sp}\alpha} + V^{2}_{\mathbf{sp}\beta}}\right) \tag{19}$$

From the PW currents' expressions, the PW current dynamics in the $(\boldsymbol{\alpha}, \boldsymbol{\beta})$ frame from Eq. (13) is:

$$\boldsymbol{I}_{\mathbf{sp}} = K\left(K_{11}\boldsymbol{\varphi}_{\mathbf{sp}} + K_{12}\boldsymbol{\varphi}_{\mathbf{sc}} + K_{13}\boldsymbol{\varphi}_{\mathbf{r}}\right) \tag{20}$$

Then, the current dynamics becomes:

$$\frac{\mathbf{d}\boldsymbol{I}_{\mathbf{sp}}}{\mathbf{d}t} = \boldsymbol{K}\left(\boldsymbol{K}_{11}\dot{\varphi}_{\mathrm{sp}} + \boldsymbol{K}_{12}\dot{\varphi}_{\mathrm{sc}} + \boldsymbol{K}_{13}\dot{\varphi}_{\mathrm{r}}\right) \tag{21}$$

where $\dot{\boldsymbol{\varphi}}_{\mathbf{sp}}$, $\dot{\boldsymbol{\varphi}}_{\mathbf{sc}}$ and $\dot{\boldsymbol{\varphi}}_{\mathbf{r}}$ are the derivatives of $\boldsymbol{\varphi}_{\mathbf{sp}}$, $\boldsymbol{\varphi}_{\mathbf{sc}}$ and $\boldsymbol{\varphi}_{\mathbf{r}}$ and obtained from Eqs. (2) to (4), thus:

$$\begin{aligned}\frac{\mathbf{d}\boldsymbol{I}_{\mathbf{sp}}}{\mathbf{d}t} &= D_1\left(\boldsymbol{V}_{\mathbf{sp}} - R_{\mathrm{sp}}\boldsymbol{I}_{\mathbf{sp}}\right) + D_2\left(\boldsymbol{V}_{\mathbf{sc}} + jp_{\mathrm{p}}\omega_{\mathrm{r}}\boldsymbol{\varphi}_{\mathbf{r}} - R_{\mathrm{r}}\boldsymbol{I}_{\mathbf{r}}\right)\\ &\quad + D_3\left(-R_{\mathrm{sc}}\boldsymbol{I}_{\mathbf{sc}} + j\left(p_{\mathrm{p}} + p_{\mathrm{c}}\right)\omega_{\mathrm{r}}\boldsymbol{\varphi}_{\mathbf{sc}}\right)\end{aligned} \tag{22}$$

with $D_1 = KK_{11}$, $D_2 = KK_{13}$, $D_3 = -KK_{12}$, $\boldsymbol{I}_{\mathbf{r}} = \frac{1}{M_{\mathrm{p}}}\left(\boldsymbol{\varphi}_{\mathbf{sp}} - L_{\mathbf{sp}}\boldsymbol{I}_{\mathbf{sp}}\right)$ and

$$\boldsymbol{\varphi}_{\mathbf{r}} = \frac{L_{\mathbf{r}}}{M_{\mathrm{p}}}\left(\boldsymbol{\varphi}_{\mathbf{sp}} - L_{\mathbf{sp}}\boldsymbol{I}_{\mathbf{sp}}\right) + M_{\mathbf{p}}\boldsymbol{I}_{\mathbf{sp}} + M_{\mathbf{c}}\boldsymbol{I}_{\mathbf{sc}}.$$

Giving the current dynamic as a function on the form

$$\frac{\mathbf{d}\boldsymbol{I}_{\mathbf{sp}}}{\mathbf{d}t} = F\left(\boldsymbol{I}_{\mathbf{sp}}, \boldsymbol{I}_{\mathbf{sc}}, \boldsymbol{V}_{\mathbf{sp}}, \boldsymbol{V}_{\mathbf{sc}}, \boldsymbol{\varphi}_{\mathbf{sp}}\right) \tag{23}$$

and taking into account the sampling period T_{s}, the PW current prediction equation at a given $k+1$ time instant from k time instant using discretization of the previous dynamic equation gives:

$$\boldsymbol{I}^{k+1}_{\mathbf{sp}} = \boldsymbol{I}^{k}_{\mathbf{sp}} + T_{\mathrm{s}}F\left(\boldsymbol{I}_{\mathbf{sp}}, \boldsymbol{I}_{\mathbf{sc}}, \boldsymbol{V}_{\mathbf{sp}}, \boldsymbol{V}_{\mathbf{sc}}, \boldsymbol{\varphi}_{\mathbf{sp}}\right) \tag{24}$$

Then from this equation and the established references Eqs. (18) and (19), the cost function can be tuned from the expression:

$$C_f = \left|I_{\mathrm{sp}\alpha_{\mathrm{ref}}} - Re\left(\boldsymbol{I}^{k+1}_{\mathbf{sp}}\right)\right|^{2} + \left|I_{\mathrm{sp}\beta_{\mathrm{ref}}} - Im\left(\boldsymbol{I}^{k+1}_{\mathbf{sp}}\right)\right|^{2} \tag{25}$$

In the present control strategy, the aim is to determine the voltages that minimize C_f. Here, a two-level voltage source inverter (VSI) is used for an overall of eight voltages with two of them null. Figure 1 represents the schematic diagram of the proposed control strategy.

3.3 Sliding Mode Power Predictive Control

3.3.1 Sliding Mode Control principle

Sliding mode control (SMC) is a class of variable structure control (VSC) schemes known to be less sensitive to disturbances and parameter variations. They are used to constrain the system to stay on a defined or desired manifold.

Here is considered a class of systems described by equation:

$$\dot{x} = f(x,t) + B(x,t).u(x,t) \tag{26}$$

where $\boldsymbol{x} \in \mathbb{R}^{\boldsymbol{n}}$ (state vector), u is the control vector $\boldsymbol{u} \in \mathbb{R}^{\boldsymbol{n}}$, $\boldsymbol{f}(\boldsymbol{x},\boldsymbol{t}) \in \mathbb{R}^{\boldsymbol{n}}$ and $\boldsymbol{B}(\boldsymbol{x},\boldsymbol{t}) \in \mathbb{R}^{\boldsymbol{n}\times\boldsymbol{m}}$.

Therefore, it is possible to define a set S_{s} of the state trajectories $\boldsymbol{x}$, called sliding surface such as:

$$\mathrm{S}_{\mathrm{s}} = \{x(t)|\sigma(x,t)\} \tag{27}$$

Let's note that one of the most used surfaces is that of Slotine (Slotine and Sastry 1983) described by:

$$\sigma(x,t) = \left(\frac{\mathrm{d}}{\mathrm{d}t} + \lambda\right)^{n-1} e_r \tag{28}$$

where n is the system's order, λ a positive constant and e_r the error vector (difference between the desired values and the obtained values)

In the classic SMC, two conditions must be satisfied:

$$\sigma(x,t) = 0 \text{ and } \dot{\sigma}(x,t) = 0 \tag{29}$$

Hence, the control laws satisfying them are written in the form:

$$u = u^{\mathrm{eq}} + u^{n} = u^{\mathrm{eq}} - k_s * \mathrm{sgn}(\sigma(x,t)) \tag{30}$$

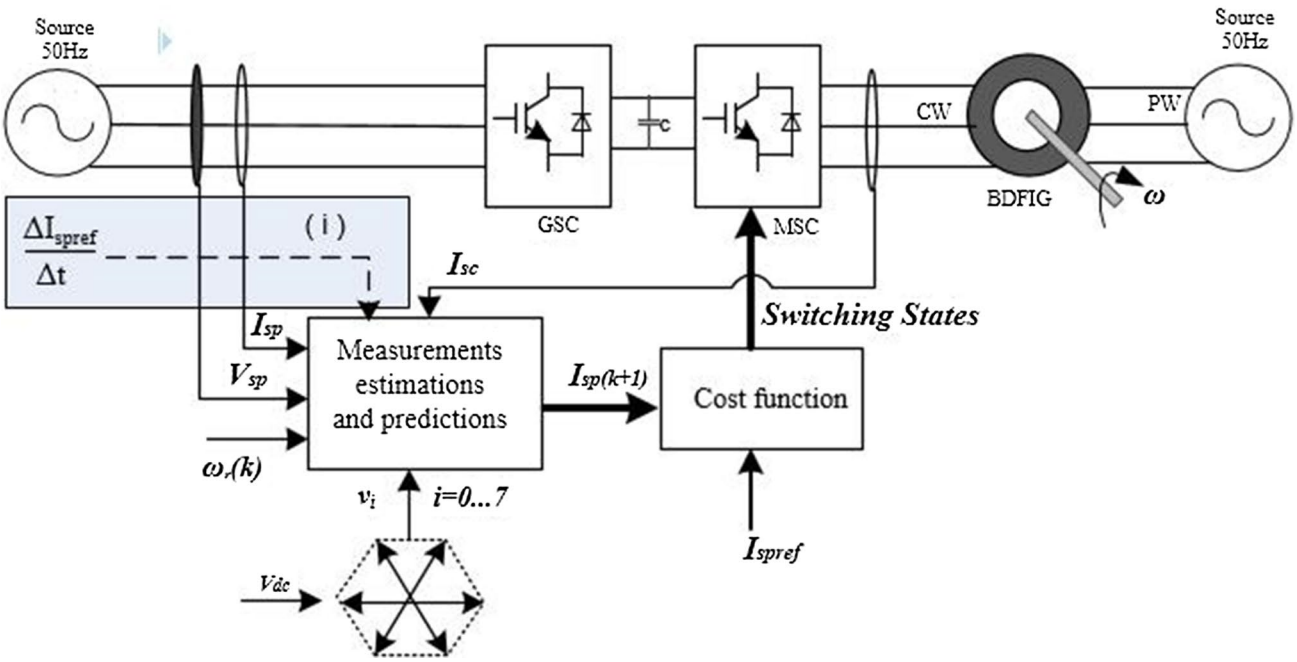

Fig. 1 Schematic diagram of the proposed control schemes; (i) needed for SMPPC

where u^{eq} is the equivalent control vector and u^n is the switching part of the control, while k_s is the gain of the controller strictly positive.

3.3.2 Particle Swarm Optimization Algorithm

Particle Swarm Optimization (PSO) algorithm (Fig. 2) introduced by James and Russel (1995) is a stochastic and iterative evolutionary-type method with fast convergence. The PSO algorithm for continuous nonlinear optimization problems was found robust (Zwe-Lee Gaing 2004) and superior to other stochastic methods (Zwe-Lee Gaing 2004; Hiswe et al. 2019). It uses a population of individuals where each particle adjusts its flight according to its experience and the ones of its companions (Yuhui and Russel 1998). The following Eq. (31) describes the update of the speed and the position of each particle:

$$\begin{cases} V_{i+1} = \mu_1 V_i + \mu_2 (x_{ip} - x_i) + \mu_3 (x_g - x_i) \\ x_{i+1} = x_i + V_{i+1} \end{cases} \quad (31)$$

where $\mu_1, \mu_2, \mu_3 \in [0, 1]$; x_{ip} and x_g are, respectively, for an ith particle and the swarm the best position from the first position and the best global position.

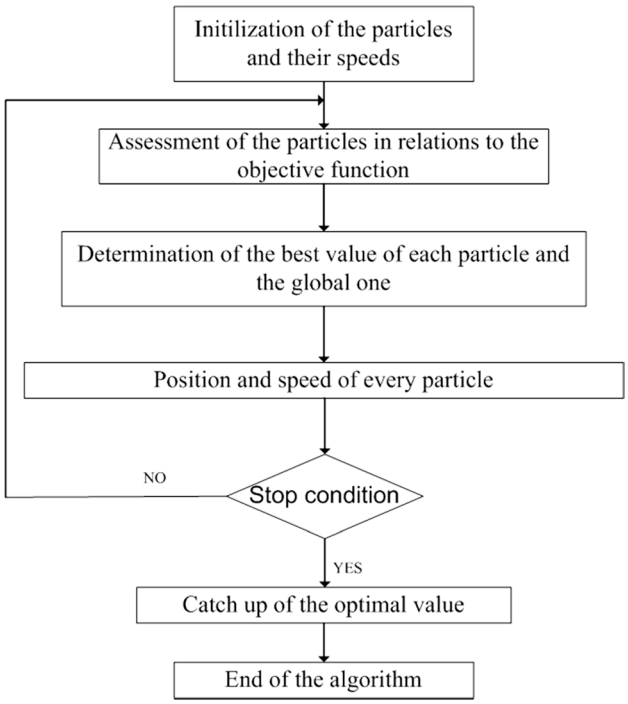

Fig. 2 PSO flowchart

3.3.3 Proposed Sliding Mode Power Predictive Control (SMPPC)

In this section, some of preview equations will be used. In that sense, the system described by Eq. (26) will be considered as the same in Eq. (14). The aim is to use the control strategy in Sect. 3.2 to define a new one choosing as sliding surface the PW currents in the $\alpha\beta$ frame. Hence, Eq. (28) becomes:

$$S_s = \left(\frac{d}{dt} + k_I\right)^{n-1}\left(I_{spref} - I_{sp}\right) \tag{32}$$

where k_I is a positive constant as previously said and which has to be thoroughly determined in order to force the error to tend to zero.

In our case, $n=2$ leading to the following:

$$S_s = \left(\frac{dI_{spref}}{dt} + \frac{dI_{sp}}{dt}\right) + k_I\left(I_{spref} - I_{sp}\right) \tag{33}$$

where $\frac{dI_{sp}}{dt}$ is given in Eq. (22).

Therefore, taking into account Eq. (24) where current can be predicted, this enables us to define a new cost function Eq. (34) which has to be minimized according to the selected voltage among the eight possibilities of the two-level inverter:

$$C_f = \left|Re\left(S_s\right)\right|^2 + \left|Im\left(S_s\right)\right|^2 \tag{34}$$

4 Simulation Results and Discussion

The SMPPC presented in the previous section uses the principle of the I-MPPC. The PSO algorithm was used to optimize the result of the SMPPC since the Lyapunov stability condition gives just a range of the control parameter k_I. Hence, an objective function minimizing the integral absolute errors (Eq. 35) is defined:

$$OF_{ITAE} = \int_0^{t_{sim}} |e_r| dt \tag{35}$$

where t_{sim} is the simulation time and e_r is the error between the desired and the measured powers. The objective function of the preview parameter k_I ensuring a convergence and a stability of the control is depicted in Fig. 3.

4.1 Performances Under Step Variations

Simulation results of control strategies are carried out in per units (pu) on a BDFIG which parameters are given in Table 1. The PW is supplied on each phase by a 220 V constant voltage. The sampling period is $T_s = 50$ µs, the DC-link voltage is 540 V, and the shaft speed is set at 0.86 pu. The active power moves from 0 pu to − 1 pu at 1.5 s and then steps again from the last value to the first at 2.3 s, while the reactive power steps from 0 to 1 pu at 1.7 s and from 1 to 0 pu at 2.1 s.

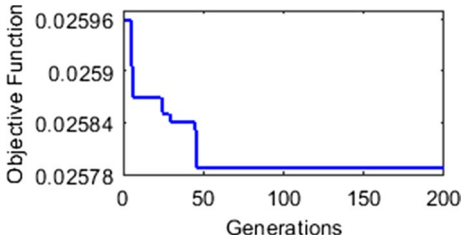

Fig. 3 PSO algorithm objective function convergence

Figure 4 gives tracking response of the system for the proposed controls during step changes compared to the DPC proposed in Jiefeng et al. (2014). The three methods show good tracking of the desired values despite the high amount of ripples observed with the DPC as it can be seen in Table 2 giving THDs, ripples and rising and descending time (t_r and t_d).

The proposed schemes (SMPPC and I-MPPC) according to quantities evaluated in Table 2 present lower THDs and power ripples than the DPC. In fact, one of the main drawbacks of the DPC is its high amount of ripples which does not make it affordable when power quality is privileged. The amount of ripples of the reactive power, for example, is almost divided by two under SMPPC. Both SMPPC and I-MPPC could be accurate for a BDFIG power control, but much better with the SMPPC which could be adequate to have less polluted grid thanks to THD values. However, in terms of rising and descending times the I-MPPC appears to be faster than the SMPPC. Else, brief peaks are observed during reference changes of active power on reactive power and vice versa in SMPPC and I-MPPC which is not the case with the DPC. To avoid those effects, a way is to operate step by step with small values. Globally, with these control schemes, active power or reactive power can be independently controlled.

Table 1 Parameters values

	PW	CW	Rotor
Resistance (Ω)	1.732	1.079	0.476
Self-inductance (H)	0.7148	0.1217	0.1326
Mutual inductance (H)	0.2421	0.0598	
Pole pair numbers	1	3	

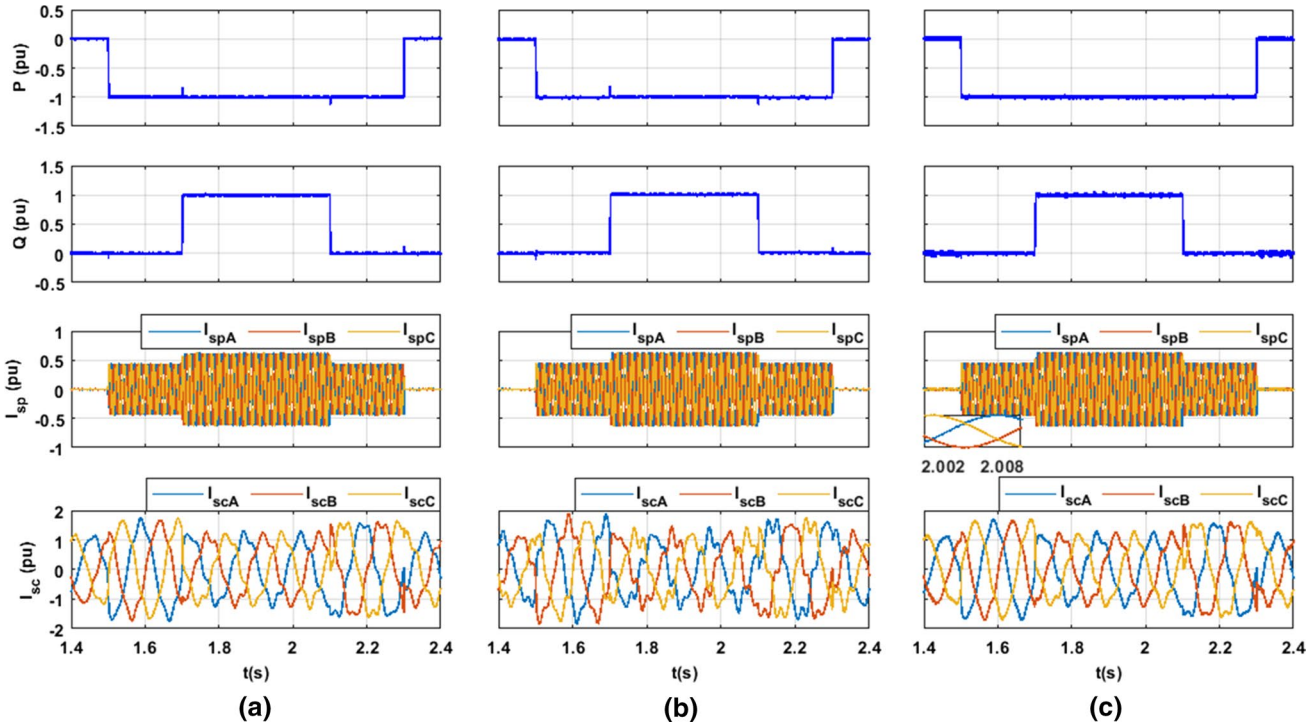

Fig. 4 Active power, reactive power, PW currents and CW currents under step change **a** SMPPC, **b** I-MPPC, **c** DPC

Table 2 Simulation result quantities

	P			Q			Isp
	t_d (ms)	t_r (ms)	ΔP_{rip} (%)	t_d (ms)	t_r (ms)	ΔQ_{rip} (%)	THD (%)
DPC (Jiefeng et al. 2014)	1.32	1.00	9.84	2.03	2.30	12.15	1.87
I-MPPC (this work)	2.14	1.10	7.56	1.31	1.96	7.32	1.28
SMPPC (this work)	1.8	1.15	6.56	1.40	1.72	6.65	1.25

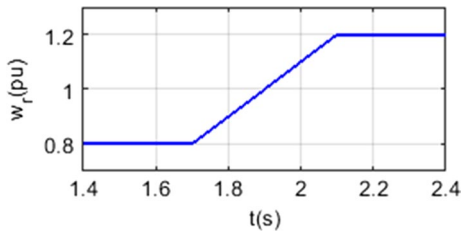

Fig. 5 Rotor speed variation

4.2 Test of Robustness

4.2.1 Test Under Speed and Machine Parameters Variation

In order to evaluate other performances of the control schemes, the BDFIG is submitted to a speed variation as shown in Fig. 5 following a ramp from 0.8 to 1.2 pu. The active power is set to –1 pu, while the reactive power is null (Fig. 6). Good tracking (Fig. 6) of the desired values of the active and reactive powers for both I-MPPC and SMPPC is kept leading to the robustness to speed variations. The effect when crossing the synchronous speed (750 rpm) which implies the decrease in the CW frequency is also observed and does not affect the desired powers which are normally controlled.

Further performances of the BDFIG under the proposed control schemes are evaluated in resistances variations and little mutual inductance variations (which can occur because of heat, magnetic saturation or severe conditions of operation, etc.). A +50% change on PW, CW and rotor resistances and a +5% on mutual inductances are applied (Fig. 7). Here, step changes are operated on active power from − 1 to − 0.5 pu at 1.6 s and from − 0.5 to − 1 pu at 2.3 s, while reactive power moves from 0 to 0.5 pu at 1.7 s and from 0.5 to 1 pu at 2.1 s. It can be observed that good dynamics and static behaviours are kept although ripples are more pronounced when the parameter values

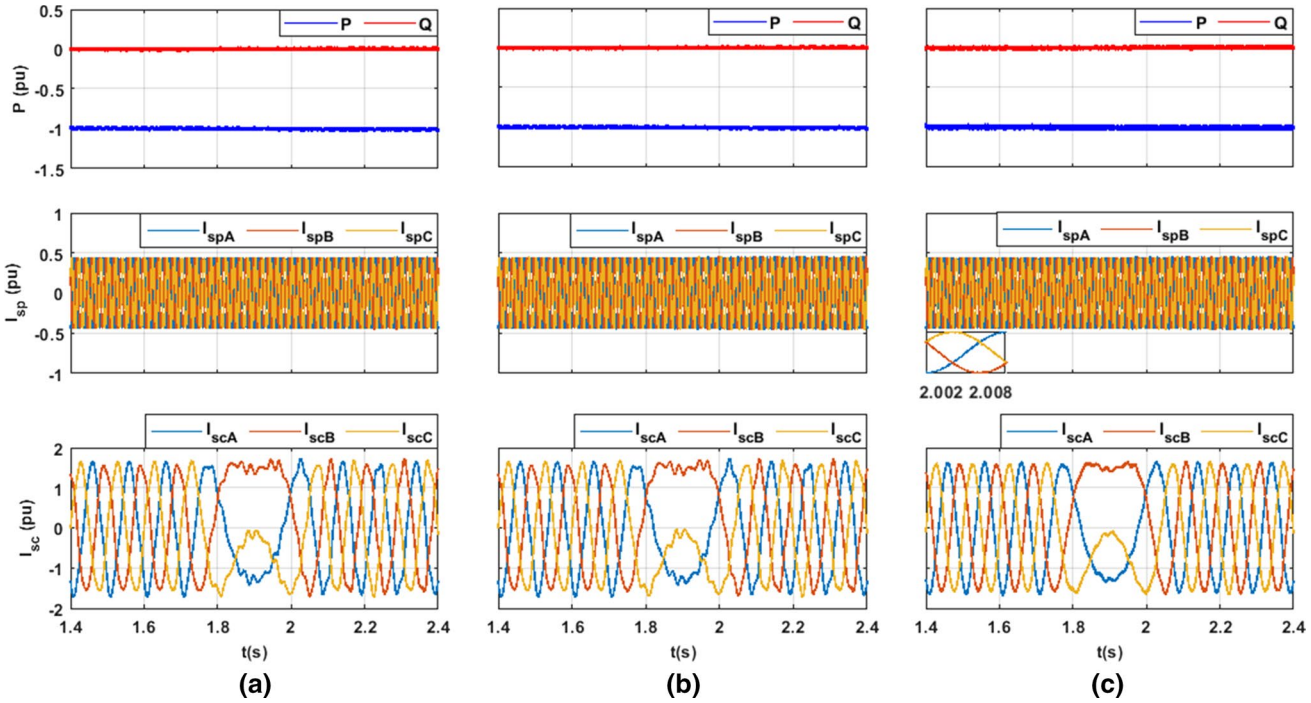

Fig. 6 Active power, reactive power, PW currents and CW currents under speed variation **a** SMPPC, **b** I-MPPC, **c** DPC

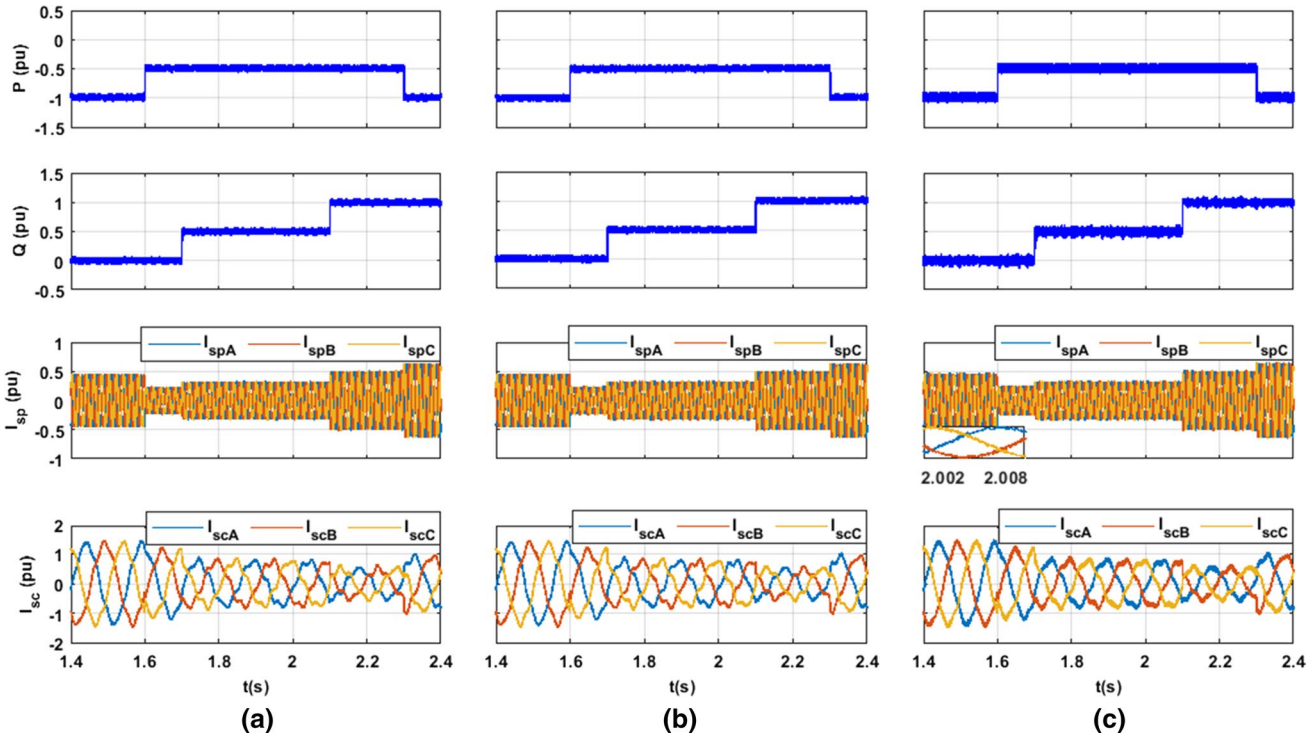

Fig. 7 Active power, reactive power, PW currents and CW currents under resistances variation (+50%) and mutual inductances variation (+5%) **a** I-MPPC, **b** MPPC, **c** DPC

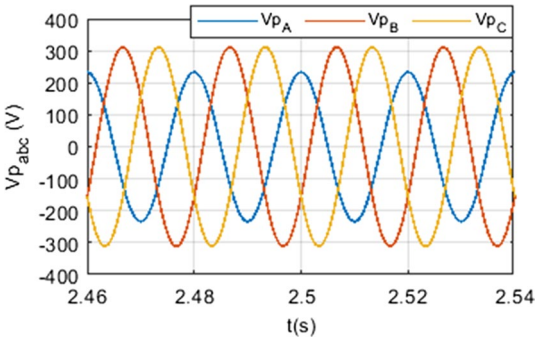

Fig. 8 Unbalanced grid voltage

are increased. However, those ripples are visually higher with DPC than SMPPC and I-MPPC.

Both rotor speed variation and resistances variations have negligible or insignificant effects on desired values under the proposed control strategies.

4.2.2 BDFIG Under Unbalanced Grid Voltage Conditions

Given an unbalanced three-phase system, it can be decomposed into three three-phase systems called zero sequence, positive (direct) sequence and negative (indirect) sequence all balanced and symmetric. Hence in the case of the BDFIG, the zero sequence of the currents and the voltages is zero. Therefore in the $\alpha\beta$ frame, a quantity X is described as in Eq. (36):

$$X_{\alpha\beta}(t) = X^{+}_{\alpha\beta}(t) + X^{-}_{\alpha\beta}(t) = X^{+}_{\alpha\beta}.e^{j(\omega t+\varphi_{+})} + X^{-}_{\alpha\beta}.e^{-j(\omega t+\varphi_{-})} \tag{36}$$

where X is either the current or the voltage and φ_{+} and φ_{-} are the phase shift for positive (+) and negative (−) sequence components. The technique to extract various components is also given in Lie et al. (2005) and expressed as follows:

$$\begin{aligned} X^{+}_{\alpha\beta}(t) &= 0.5\big(X_{\alpha\beta}(t) + j\cdot X_{\alpha\beta}(t - T/4)\big) \\ X^{-}_{\alpha\beta}(t) &= 0.5\big(X_{\alpha\beta}(t) - j\cdot X_{\alpha\beta}(t - T/4)\big) \end{aligned} \tag{37}$$

Here, T is the signal fundamental frequency period.

In the present section, a 25% drop voltage on one phase is considered as shown in Fig. 8. Despite the good tracking of the desired powers (Fig. 9), the THDs (Table 3) clearly show how distorted and unbalanced the PW currents can be. To correct these currents, power compensation presented in Jiefeng et al. (2014) and summarized in Fig. 10 is used to obtain sinusoidal and balanced currents. This consists in eliminating the negative sequence of the PW current which appears when the grid voltage becomes unbalanced.

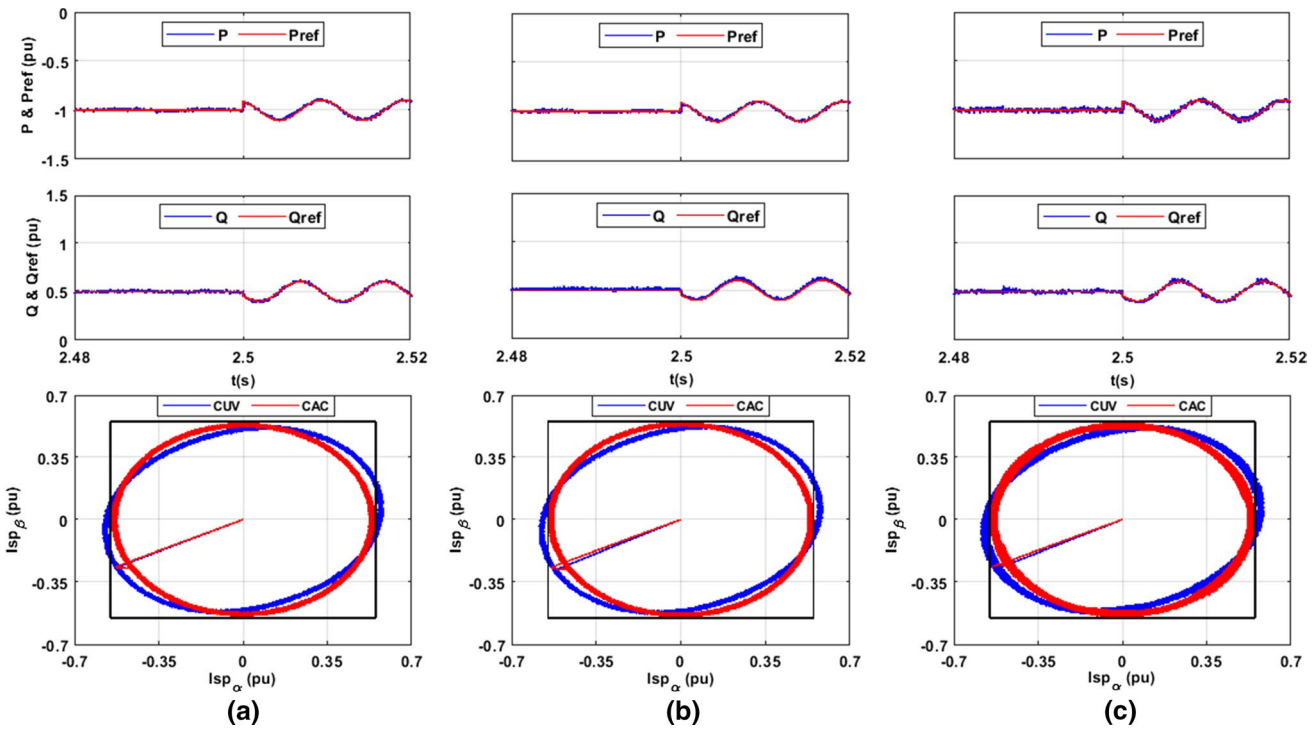

Fig. 9 Active power, reactive power and PW currents under unbalanced grid voltage condition and power compensation **a** SMPPC, **b** I-MPPC, **c** DPC. (*CUV: currents under unbalanced voltage; CAC: currents after compensation*)

Table 3 PW current THDs before compensation (BC) and after compensation (AC)

	SMPPC (this work)		I-MPPC (this work)		DPC (Jiefeng et al. 2014)	
	BC	AC	BC	AC	BC	AC
THDs (%)	9.30	1.48	9.09	1.49	9.03	2.09

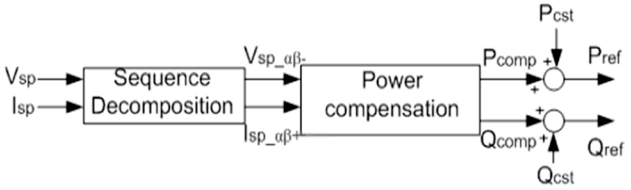

Fig. 10 Power references determination based on power compensation

There, P_{comp} and Q_{comp} are the required active and reactive power compensations, and P_{cst} and Q_{cst} are the previews needed power references, while P_{ref} and Q_{ref} are the new power references.

In Fig. 9, before compensation (that is before 2.5 s), active and reactive power references which are constants are well followed showing the accuracy of the control techniques. However, PW currents become unbalanced with high amount of THD leading to the "pollution" of the system. Compensation technique is therefore applied at the time 2.5 s, and the constant active and reactive powers which were constants become oscillating ones as depicted, and the tracking of references is ensured. As we can find on the PW currents represented in the $\alpha\beta$ frame, a square is used to evaluate how the currents under unbalanced grid condition without compensation and after compensation are. Thus, a balanced three-phase system in the preview will present a circle shape within a square, while an unbalanced system an ellipse which will present outer part to the square. Comparison of different figures clearly shows that the DPC will lead to severe distorted currents, which is confirmed in Table 3 by the THDs of the PW currents without and with power compensation under unbalanced grid condition. The drastic drop of THDs amount can be explained by the fact that using power compensation leads to oscillating power references. With the required powers, the SMPPC presents the lesser amount of THD than the others and a cleaner PW current could then be obtained.

5 Conclusion

A Sliding Mode Power Predictive Control (SMPPC) and an Indirect Model Power Predictive Control (I-MPPC) are proposed here for power tracking in a BDFIG and compared to the conventional DPC. These control techniques are based on current predictions obtained after defining currents' dynamic and discretization. The appropriate voltage vector is chosen among the eight vectors of a two-level inverter after the minimization of the corresponding cost function defined as the quadratic absolute current errors. With these approaches, suitable state behaviours are obtained for transient and steady state. The behaviour of the BDFIG is evaluated under some parameters variations. To strengthen its applicability for wind power generation systems, power compensation is used to obtain balanced and sinusoidal currents under an unbalanced grid condition. The SMPPC and I-MPPC offer cleaner power winding currents than the DPC in terms of THDs reduction enhancing the quality of the grid currents. The SMPPC or the I-MPPC could therefore be an alternative for power control of BDFIG by tackling especially problem of power ripples amount encountered under direct power control and grid pollution by harmonics due to high amount of THDs.

Appendix A

$$K = 1/\left(L_{sp}L_{sc}L_r - L_{sc}M_p^2 - L_{sp}M_c^2\right)$$

$$K_{11} = L_{sc}L_r - M_c^2;\ K_{12} = K_{21} = M_pM_c;\ K_{13} = K_{13} = -L_{sc}M_p$$

$$K_{22} = L_{sp}L_r - M_p^2;\ K_{23} = K_{32} = -L_{sp}M_c;\ K_{33} = L_{sc}L_p$$

Appendix B

$$\epsilon_{11} = -KK_{11}R_{sp} - KK_{33}R_r - jp_pL_{sc}KK_{22}\omega_r + j(p_p + p_c)K_{23}M_c\omega_r$$

$$\epsilon_{12} = KK_{12}R_{sc} - jp_pM_cKK_{13}\omega_r$$

$$\epsilon_{13} = KL_{sc}R_r - jp_pL_{sc}L_rK\omega_r + j(p_p + p_c)KM_c^2\omega_r$$

$$\epsilon_{21} = KK_{12}R_{sp} + KK_{23}\frac{L_{sp}L_r}{M_p} - jp_cK\omega_r\left(-\frac{L_{sp}L_r}{M_p}K_{23} - K_{12}L_{sp}\right)$$

$$\epsilon_{22} = -KK_{22}R_{sc} + jp_pKK_{23}M_c\omega_r + j(p_p + p_c)KK_{22}L_{sc}$$

$$\epsilon_{23} = KK_{23}\frac{R_r}{M_p} + jp_pKK_{12}\omega_r$$

$$\epsilon_{31} = -R_{sp}$$

$$\epsilon_{32} = \epsilon_{33} = 0$$

$$\varepsilon_{11} = KK_{11};\ \varepsilon_{12} = -KK_{12};\ \varepsilon_{21} = \varepsilon_{12} = -KK_{12};$$

$$\varepsilon_{22} = \varepsilon_{11} = KK_{11};\ \varepsilon_{13} = \varepsilon_{23} = \varepsilon_{31} = \varepsilon_{32} = \varepsilon_{33} = 0.$$

References

David, S.-M., Jose, L. R.-A., & Santiago, A. (2008). Direct power control applied to doubly fed induction generator under unbalanced grid voltage conditions. *IEEE Transactions on Power Electronics, 23*(5), 2328–2336. https://doi.org/10.1109/tpel.2008.2001907.

Eduard, M., Batan, T., Deniz, Y., Charles, P. B. (1999). Understanding the unbalanced-voltage problem in wind turbine generation. In *Conference record of the 1999 IEEE Industry applications conference. Thirty-forth IAS annual meeting,* Phoenix, AZ, USA, doi:10.1109/ias.1999.801678.

Francisco, B., Carlos, V., Dionisio, R., & Carlos, A. P. (2009). Characterization of the rotor magnetic field in a brushless doubly-fed induction machine. *IEEE Transactions on Energy Conversion, 24*(3), 599–607. https://doi.org/10.1109/TEC.2009.2025345.

Gaing, Z.-L. (2004). A particle swarm optimization approach for optimum design of PID controller in AVR system. *IEEE Transactions on Energy Conversion, 19*(2), 5. https://doi.org/10.1109/tec.2003.821821.

Gonzalo, A., Miguel, A. R., Grzegorzi, I., & Javier, P. (2010). Direct power control of doubly-fed-induction-generator-based wind turbine under unbalanced grid voltage. *IEEE Transactions on Power Electronics, 25*(2), 442–452. https://doi.org/10.1109/tpel.2009.2027438.

Guanguan, Z., Jian, Y., Yao, S., Mei, S., Weiyi, T., Qi, Z., et al. (2017). A robust control scheme based on ISMC for the brushless doubly fed induction machine. *IEEE Transactions on Power Electronics, 33*(4), 3129–3140. https://doi.org/10.1109/tpel.2017.2708741.

Hadi, J., & Hanieh, K. (2017). BIST-based testing and diagnosis of LUTs in SRAM-based FPGAs. *Emerging Science Journal*. https://doi.org/10.28991/ijse-01125.

Henk, P., Jan, A. F., Bogi, B. J., Asger, B. A., Kais, A., & Richard, A. M. (2013). Trends in wind turbine generator systems. *IEEE Journal of Emerging and Selected Topics in Power Electronics, 1*(3), 174–185. https://doi.org/10.1109/jestpe.2013.2280428.

Hiswe, F., Effa, J. Y., & Kenmoe, F. E. D. (2019). Optimization of sensorless field-oriented control of an induction motor taking into account of magnetic saturation. *International Jounal of Dynamics and Control*. https://doi.org/10.1007/s40435-018-00503-8.

James K., & Russel, E. (1995). Particle swarm optimization. In *Proceedings of ICNN'95—international conference on neural networks*, Perth, WA, Australia.

Javier, P., Estanis, O., Daniel, R., & Miguel, R. (2006). Unified reference frame dq model of the brushless doubly fed machine. *IEE Proceedings-Electric Power Applications, 153*(5), 726–734. https://doi.org/10.1049/ip-epa:20050404.

Javier, P., Estanis, O., Izaksun, S., & Miguel, R. (2009). Vector control design and experimental evaluation for the brushless doubly fed machine. *IET Electric Power Applications, 3*(4), 247–256. https://doi.org/10.1049/iet-epa.2008.0090.

Jiabing, H., Heng, N., Bin, H., Yikang, H., & Zi, Q. Z. (2010). Direct active and reactive power regulation of DFIG using sliding-mode control approach. *IEEE Transactions on Energy Conversion, 25*(4), 1028–1039. https://doi.org/10.1109/tec.2010.2048754.

Jianping, G., Wei, X., Yi, L., & Kailiang, Y. (2018). Improved control scheme for unbalanced standalone BDFIG using dead beat control method. In *2018 IEEE energy conversion congress and exposition (ECCE),* Portland, OR, USA, https://doi.org/10.1109/ecce.2018.8557660.

Jiansheng, C., Wei, Z., Bojia, C., & Yunlong, M. (2015). Improved vector control of brushless doubly fed induction generator under unbalanced grid conditions for offshore wind power generation. *IEEE Transactions on Energy Conversion, 31*(1), 293–302. https://doi.org/10.1109/tec.2015.2479859.

Jiefeng, H., Jianguo, Z., & David, G. D. (2014). A new control method of cascaded brushless doubly fed induction generators using direct power control. *IEEE Transactions on Energy Conversion, 29*(3), 771–779. https://doi.org/10.1109/tec.2014.2325046.

Jose, R., & Patricio, C. (2012). *Predictive control of power converters and electrical drives*. Universidad Tecnica Federico Santa Maria, Valparaiso, Chile: Wiley.

Lie, X., Bjarne, R. A., & Phillip, C. (2005). VSC transmission operating under unbalanced AC conditions: Analysis and control design. *IEEE Transactions on Power Delivery, 20*(1), 427–434. https://doi.org/10.1109/tpwrd.2004.835032.

Maryam, M., Rasool, K., & Mohammad-Reza, A. (2016). Model-based predictive direct power control of brushless doubly fed reluctance generator for wind power applications. *Alexandria Engineering Journal, 55*(3), 2497–2507. https://doi.org/10.1016/j.aej.2016.08.004.

Ming, C., & Yiing, Z. (2014). The state of the art of wind energy conversion systems and technologies: A review. *Energy Conversion and Management, 88,* 332–347. https://doi.org/10.1016/j.enconman.2014.08.037.

Mohamed, A. M., Said, D., Mohamed, A. S., & Ridha, C. (2017). Sliding mode control of grid connected brushless doubly fed induction generator driven by wind turbine in variable speed. *International Journal of System Assurance Engineering and Management, 8*(2), 788–798. https://doi.org/10.1007/s13198-016-0524-1.

Ramtin, S., Seyed, M. M., Mohammad, A., KashkooliM, R. A., & Sul, A. (2018). Super-twisting sliding mode direct power control of brushless doubly fed induction generator. *IEEE Transactions on Industrial Electronics*. https://doi.org/10.1109/tie.2018.2818672.

Richard, A. M., Paul, C. R., Xiaoyan, W., & Peter, J. T. (2006). Performance of BDFM as generator and motor. *IEE Proceedings-Electric Power Applications, 153*(2), 289–299. https://doi.org/10.1049/ip-epa:20050289.

Saber, K., Mehran, Z., & Pouya, D.-B. (2018). Analysis of bifurcations in a wind turbine system based on DFIG. *Emerging Science Journal*. https://doi.org/10.28991/esj-2018-01126.

Sergio, T., Marco, R., & José, L. E. (2016). Overview of wind energy conversion systems development, technologies and power electronics research trends. In *2016 IEEE internal conference on automatica (ICA-ACCA)*, Curico,Chile, https://doi.org/10.1109/ica-acca.2016.7778454.

Shiyi, S., Ehsan, A., Farhad, B., & Richard, M. (2009). Stator-flux-oriented vector control for brushless doubly fed induction generator. *IEEE Transactions on Industrial Electronics, 56*(10), 4220–4228. https://doi.org/10.1109/tie.2009.2024660.

Shiyi, S., Teng, L., Ehsan, A., & Richard, A. M. (2013). Dynamic control of the brushless doubly fed induction generator under unbalanced operation. *IEEE Transactions on Industrial Electronics, 60*(6), 2465–2476. https://doi.org/10.1109/tie.2012.2211313.

Slotine, J. J., & Sastry, S. (1983). Tracking control of nonlinear systems using sliding surfaces, with application to robot manipulators. *International Journal of Control, 38*(2), 465–492. https://doi.org/10.23919/acc.1983.4788090.

Stephen, W., Antonio, C. F., & Alan, K. W. (1997). Generalised theory of the brushless doubly-fed machine, part 1: Analysis. *IEE Proceedings-Electric Power Applications, 144*(2), 111–122. https://doi.org/10.1049/ip-epa:19971051.

Tim, D. S., Henk, P., & Jan, A. F. (2016). Brushless doubly-fed induction machines for wind turbines: Developments and research challenges. *IET Electric Power Applications, 11*(6), 991–1000. https://doi.org/10.1049/iet-epa.2016.0118.

Tohidi, S. (2016). Analysis and simplified modelling of brushless doubly-fed induction machine in synchronous mode of operation. *IET Electric Power Applications, 10*(2), 110–116. https://doi.org/10.1049/iet-epa.2015.0217.

Venkata, Y., Bin, W., Paresh, C. S., Samir, K., & Mehdi, N. (2015). High-power wind energy conversion systems: State-of-the-art and emerging technologies. *Proceedings of the IEEE, 103*(5), 740–788. https://doi.org/10.1109/jproc.2014.2378692.

Xiaoyu, L., Qiuming, L., Shishu, X., & Zhenqing, L. (2018). Numerical study of the wake flow of a wind turbine with consideration of the inflow turbulence. *Civil Engineering Journal*. https://doi.org/10.28991/cej-03091125.

Xinchi, W., Ming, C., Wei, H., Zhu, J., & Haitao, Y. (2017). Model predictive power control of a brushless doubly fed twin stator induction generator. In *20th International conference on electrical machines and systems (ICEMS)*, https://doi.org/10.1109/ecce.2017.8096856.

Xuan, L., Tao, P., Hanbing, D., Guanguan, Z., & Pat, W. (2017). A modulated model predictive control scheme for the brushless doubly-fed induction machine. In *Energy conversion congress and exposition (ECCE)*, Cincinnati, OH, USA, https://doi.org/10.1109/ecce.2017.8095945.

Yuhui, S. & Russel, E. (1998). A modified particle swarm optimizer. In *Proceedings of the IEEE conference on Evolutionary computation, ICE*.